Background error covariance with balance constraints for aerosol species and applications in variational data assimilation

Zengliang Zang[1], Zilong Hao[1], Yi Li[1], Xiaobin Pan[1], Wei You[1], Zhijin Li[2] and Dan Chen[3]

Units: [1] College of Meteorology and Oceanography, PLA University of Science and Technology, Nanjing 211101, China;

[2]Joint Institute For Regional Earth System Science and Engineering, University of California, Los Angeles, California90095, USA;

[3]National Center for Atmospheric Research, Boulder, Colorado 80305, USA

June 8, 2016

Corresponding author:
Prof. Zengliang Zang
E-mail: zzlqxxy@163.com
Telephone: 86-025-80830400
Fax: 86-025-80830400
Address: No.60, Shuanglong Street, Nanjing 211101, China

Abstract

Balance constraints are important for background error covariance (BEC) in data assimilation to spread information between different variables and produce balance analysis fields. Using statistical regression, we develop a balance constraint for the BEC of aerosol variables and apply it to a three-dimensional variational data assimilation system in the WRF/Chem model. One-month forecasts from the WRF/Chem model are employed for BEC statistics. The cross-correlations between the different species are generally high. The largest correlation occurs between elemental carbon and organic carbon with as large as 0.9. After using the balance constraints, the correlations between the unbalanced variables reduce to less than 0.2. A set of data assimilation and forecasting experiments is performed. In these experiments, surface $PM_{2.5}$ concentrations and speciated concentrations along aircraft flight tracks are assimilated. The analysis increments with the balance constraints show spatial distributions more complex than those without the balance constraints, which is a consequence of the spreading of observation information across variables due to the balance constraints. The forecast skills with the balance constraints show substantial and durable improvements from the 2^{nd} hour to the 16^{th} hour compared with the forecast skills without the balance constraints. The results suggest that the developed balance constraints are important for the aerosol assimilation and forecasting.

Keyword: aerosol species, WRF/Chem, data assimilation, balance constraint, background error covariance

1. Introduction

Aerosol data assimilation in chemical transport models has received an increasing amount of attention in recent years as a basic methodology for improving aerosol analysis and forecasting. In a data assimilation system, the background error covariance (BEC) plays a crucial role in the success of an assimilation process. The BEC and the observation error determine analysis increments from the assimilation process (Derber and Bouttier 1999, Chen et al., 2013).

However, accurate estimation of the BEC remains difficult due to a lack of information about the true atmospheric states and also due to computational requirement arising from the large dimension of the BEC (typically $10^7 \times 10^7$). For a variational data assimilation system, a few methods have been developed to estimate and simplify the expression of the BEC, such as the analysis of innovations, the NMC (National Meteorological Center) and the ensemble-based (Monte Carlo) methods. The NMC method is extensively used in operational atmospheric and meteorology-chemistry data assimilation systems. It assumes that the forecast errors are approximated by differences between pairs of forecasts that are valid at the same time (Parrish and Derber, 1992). Pagowski et al. (2010) estimated the BEC of $PM_{2.5}$ (particles having an aerodynamic diameter less than 2.5 μm) by calculating the differences between the forecasts of 24 and 48 h, and used the estimated BEC in a Grid-point Statistical Interpolation (GSI) system (Wu et al., 2002). Benedetti et al. (2007) estimated the BEC of the sum of the mixing ratios of all aerosol species for an operational analysis and forecast systems at ECMWF (The European Centre for Medium-Range Weather Forecasts). The BEC with multiple species and size bins of aerosols have been calculated and employed in data assimilation. Liu et al. (2011) estimated the BEC with 14 aerosol species in the Goddard Chemistry Aerosol Radiation and Transport scheme of the Weather Research and Forecasting/Chemistry (WRF/Chem) model and applied it to the GSI system. Schwartz et al. (2012) increased the number of the species to 15 based on the study of Liu et al. (2011). Li et al. (2013) estimated the BEC for five species derived from the Model for Simulation Aerosol Interactions and Chemistry (MOSAIC) scheme.

One important role that the BEC plays in meteorological data assimilation is to spread information between different variables to produce balanced analysis fields, which employ balance constraints to convert original variables into new independent variables. Balance

constraints have been employed in atmospheric and oceanic data assimilation, such as geostrophic balance or temperature-salinity balance (Bannister, 2008a, 2008b). To incorporate balance constraints, the model variables are usually transformed to balanced and unbalanced parts. The unbalanced parts as control variables are can be assumed independent, and the balanced parts are constrained by balance constraints (Derber and Bouttier, 1999). Instead of using an empirical function as a balance constraint, balance constraints are also derived using regression techniques (Ricci and Weaver, 2005). Although distinct empirical relations between some variables (such as temperature and humidity) may not exist, the regression equation can also be estimated as balance constraints (Chen et al., 2013).

In current aerosol variational data assimilation with multiple variables, balance constraints are not yet incorporated in the BEC. The state variables are assumed to be independent variables without cross-correlation. However, the aerosol species are frequently highly correlated due to their common emission sources and diffusion processes. For example, the correlations in terms of the R-square between elemental carbon and black carbon exceed 0.6 in many locations across Asia and the South Pacific in both urban and suburban locations (Salako et al., 2012), and the correlations between different size bins, such as $PM_{2.5}$ and $PM_{10\text{-}2.5}$ (the diameter of particles being between 2.5 and 10 μm), are also generally significant (Sun et al., 2003; Geller et al., 2004). Thus, the cross-correlations between different species or size bins are necessary to produce balanced analysis fields. Cross-correlations spread the observation information from one variable to other variables, which can produce more balanced initial fields. For the data assimilation of the ensemble Kalman filter method, the BEC with balance constraints is assured (Pagowski et al., 2012; Schwartz et al., 2014), although the balance may break down because of localization.

Recently, several studies have suggested that the BEC with balanced cross-correlation should be introduced into aerosol variational data assimilation (Kahnert, 2008; Liu et al., 2011; Li et al., 2013; Saide et al., 2013). Kahnert (2008) exhibited cross-correlations of the seventeen aerosol variables from Multiple-scale Atmospheric Transport and Chemistry (MATCH) Model. He found that the statistical cross-correlations between aerosol components are primarily influenced by the interrelations between emissions and by interrelations due to chemical reactions to a much lesser degree. Saide et al., (2012; 2013) incorporated the capacity to add cross-correlations between

aerosol size bins in GSI for assimilating observations of aerosol optical depth (AOD) data. The cross-correlations between the two connecting size bins for each species were considered using recursive filters while, the cross-correlation is not considered for the other size bins that are not connecting.

In this paper, we explore incorporating cross-correlations between different species in BEC using balance constraints. The balance constraints are established using statistical regression. We apply the BEC with the balance constraints to a data assimilation and forecasting system with the MOSAIC scheme in WRF/Chem. The MOSAIC scheme includes a large number of variables with eight species, and flexibility of eight or four size bins. The scheme of four size bins is used in our studies. The four bins are located between 0.039–0.1 μm, 0.1–1.0 μm, 1.0–2.5 μm, and 2.5–10 μm, and the total mass of the first three bins are PM2.5. A 3DVAR system for the MOSAIC (4-bin) scheme has been developed by Li et al. (2013). For comparisons, we employ this 3DVAR system with the same model configurations as employed by Li et al. (2013). The data assimilation and forecasting experiments are performed with a focus on assessing the impact of cross-correlations of the BEC on analyses and forecasts.

The paper is organized as follows: Section 2 describes the 3DVAR system and the formulation of the BEC. Section 3 describes the WRF/Chem configuration and estimates the correlations among the emissions. The statistical characteristics of the BEC, including the regression coefficient of the cross-correlation, are discussed in Section 4. Using the BEC, experiments of assimilating surface $PM_{2.5}$ observations and aircraft observations are discussed in Section 5. Shortcomings, conclusions and future perspectives are presented in Section 6.

2. Data assimilation system and BEC

In this section, we present a formulation of the BEC with cross-correlation between different species using a regression technique. Then, the cost function with the new BEC is derived and the calculating factorization of the BEC is described.

The control variables of the data assimilation are obtained from the MOSAIC (4-bin) aerosol scheme in the WRF/Chem model (Zaveri et al., 2008). The MOSAIC scheme includes eight aerosol species, that is, elemental carbon or black carbon (EC/BC), organic carbon (OC), nitrate (NO_3), sulfate (SO_4), chloride (Cl), sodium (Na), ammonium (NH_4), and other inorganic mass

(OIN). Each species is separated into four bins with different sizes: 0.039–0.1 μm, 0.1–1.0 μm, 1.0–2.5 μm and 2.5–10 μm. The scheme involves 32 aerosol variables with eight species and four size bins. These variables cannot be directly introduced as control variables in an assimilation system in consideration of computational efficiency. The number of variables must be decreased prior to assimilation. Li et al. (2013) have lumped these variables into five species as control variables in the 3DVAR system. The five species consist of EC, OC, NO_3, SO_4 and OTR. Here, OTR is the sum of Cl, Na, NH_4 and OIN. Note that the data assimilation system aims to assimilate the observation of $PM_{2.5}$; only the first three of four size bins are utilized to lump as one control variable for each species.

For a 3DVAR system, the cost function (J), which measures the distance of the state vector to the background and observations, can be written as follows:

$$J(\boldsymbol{x}) = \frac{1}{2}(\boldsymbol{x} - \boldsymbol{x^b})^T \mathbf{B}^{-1}(\boldsymbol{x} - \boldsymbol{x^b}) + \frac{1}{2}(\boldsymbol{y} - \mathbf{H}\boldsymbol{x})^T \mathbf{R}^{-1}(\boldsymbol{y} - \mathbf{H}\boldsymbol{x}). \quad (1)$$

Here, $\boldsymbol{x}$ is the vector of the state variables, including EC, OC, NO_3, SO_4 and OTR; $\boldsymbol{x^b}$ is the background vector of these five species, which are generated by the MOSAIC scheme; $\boldsymbol{y}$ is the observation vector; $\mathbf{H}$ is the observation operator that maps the model space to the observation space and is assumed to be linear here; $\mathbf{R}$ is the observation error covariance associated with $\boldsymbol{y}$; and $\mathbf{B}$ is the background error covariance associated with $\boldsymbol{x^b}$. Eq. (1) is usually written in the incremental form

$$J(\boldsymbol{\delta x}) = \frac{1}{2}\boldsymbol{\delta x}^T \mathbf{B}^{-1}\boldsymbol{\delta x} + \frac{1}{2}(\mathbf{H}\boldsymbol{\delta x} - \boldsymbol{d})^T \mathbf{R}^{-1}(\mathbf{H}\boldsymbol{\delta x} - \boldsymbol{d}), \quad (2)$$

where $\boldsymbol{\delta x}$ ($\boldsymbol{\delta x} = \boldsymbol{x} - \boldsymbol{x}^b$) is the incremental state variable. The observation innovation vector is known as $\boldsymbol{d} = \boldsymbol{y} - \mathbf{H}\boldsymbol{x^b}$. The minimization solution is the analysis increment $\boldsymbol{\delta x}$, and the final analysis is $\boldsymbol{x^a} = \boldsymbol{x^b} + \boldsymbol{\delta x}$. This analysis is statistically optimal as a minimum error variance estimate (e.g., Jazwinski, 1970; Cohn, 1997).

In Eq. (1) or Eq. (2), $\boldsymbol{x^b}$ is a $(N \times m) -$ vector, where N is the number of model grid points, and m is the number of state variables. $\mathbf{B}$ is a symmetric matrix with a dimension of $(N \times m)^2$. For a high-resolution model, the number of vector $\boldsymbol{x^b}$ is on the order of 10^7. Therefore, the number of elements in $\mathbf{B}$ is approximately 10^{14}. With this dimension, $\mathbf{B}$ cannot be explicitly manipulated. To pursue simplifications of $\mathbf{B}$, we employ the following factorization

$$\mathbf{B} = \mathbf{DCD^T}, \tag{3}$$

where $\mathbf{D}$ and $\mathbf{C}$ are the standard deviation matrix and the correlation matrix, respectively. $\mathbf{D}$ and $\mathbf{C}$ can be described and separately prescribed after the factorization. $\mathbf{D}$ is a diagonal matrix whose elements include the standard deviation of all state variables in the three-dimensional grids. To reduce the computational cost, we use the average value of standard deviations that are at the same level. Thus, the standard deviation is simplified with vertical levels. $\mathbf{C}$ is a symmetric matrix, having the form

$$\mathbf{C} = \begin{bmatrix} \mathbf{C_{EC}} & \mathbf{C_{EC}^{OC}} & \mathbf{C_{EC}^{NO_3}} & \mathbf{C_{EC}^{SO_4}} & \mathbf{C_{EC}^{OTR}} \\ \mathbf{C_{OC}^{EC}} & \mathbf{C_{OC}} & \mathbf{C_{OC}^{NO_3}} & \mathbf{C_{OC}^{SO_4}} & \mathbf{C_{OC}^{OTR}} \\ \mathbf{C_{NO_3}^{EC}} & \mathbf{C_{NO_3}^{OC}} & \mathbf{C_{NO_3}} & \mathbf{C_{NO_3}^{SO_4}} & \mathbf{C_{NO_3}^{OTR}} \\ \mathbf{C_{SO_4}^{EC}} & \mathbf{C_{SO_4}^{OC}} & \mathbf{C_{SO_4}^{NO_3}} & \mathbf{C_{SO_4}} & \mathbf{C_{SO_4}^{OTR}} \\ \mathbf{C_{OTR}^{EC}} & \mathbf{C_{OTR}^{OC}} & \mathbf{C_{OTR}^{NO_3}} & \mathbf{C_{OTR}^{SO_4}} & \mathbf{C_{OTR}} \end{bmatrix}, \tag{4}$$

where $\mathbf{C_{EC}}$, $\mathbf{C_{OC}}$, $\mathbf{C_{NO_3}}$, $\mathbf{C_{SO_4}}$ and $\mathbf{C_{OTR}}$ at diagonal locations are the background error auto-correlation matrices that are associated with each species. They represent the correlation among pairs of grid points for one species. Other submatrices represent the correlations between different species, known as cross-correlations. For example, $\mathbf{C_{OC}^{EC}}$ represents the cross-correlations between EC and OC, and $\mathbf{C_{OC}^{EC}} = (\mathbf{C_{EC}^{OC}})^{\mathbf{T}}$. In Li et al. (2013), these cross-correlations were disregarded, that is, the five species are considered independently and $\mathbf{C}$ is thus a block diagonal matrix.

In this study, the cross-correlations between different species are considered by introducing control variable transforms (Derber and Bouttier, 1999; Barker, 2004; Huang, 2009). We divide the model aerosol variables into balanced components ($\boldsymbol{\delta x_b}$) and unbalanced components ($\boldsymbol{\delta x_u}$):

$$\boldsymbol{\delta x} = \boldsymbol{\delta x_b} + \boldsymbol{\delta x_u}. \tag{5}$$

Note the EC does not need to be divided. There is not unbalanced component for EC that is similar to the variable of vorticity in the data assimilation of ECMWF (Derber and Bouttier, 1999), or the variable of stream function in the data assimilation of MM5 (Barker, 2004). The transformation from unbalanced variables ($\boldsymbol{\delta x_u}$) to full variables ($\boldsymbol{\delta x}$) by the balance operator $\mathbf{K}$ is given by

$$\boldsymbol{\delta x} = \mathbf{K}\boldsymbol{\delta x_u}\,. \tag{6}$$

Eq. (6) can be written as

$$\begin{bmatrix} \boldsymbol{\delta EC} \\ \boldsymbol{\delta OC} \\ \boldsymbol{\delta NO_3} \\ \boldsymbol{\delta SO_4} \\ \boldsymbol{\delta OTR} \end{bmatrix} = \begin{bmatrix} \mathbf{I} & \mathbf{0} & \mathbf{0} & \mathbf{0} & \mathbf{0} \\ \boldsymbol{\rho_{21}} & \mathbf{I} & \mathbf{0} & \mathbf{0} & \mathbf{0} \\ \boldsymbol{\rho_{31}} & \boldsymbol{\rho_{32}} & \mathbf{I} & \mathbf{0} & \mathbf{0} \\ \boldsymbol{\rho_{41}} & \boldsymbol{\rho_{42}} & \boldsymbol{\rho_{43}} & \mathbf{I} & \mathbf{0} \\ \boldsymbol{\rho_{51}} & \boldsymbol{\rho_{52}} & \boldsymbol{\rho_{53}} & \boldsymbol{\rho_{54}} & \mathbf{I} \end{bmatrix} \begin{bmatrix} \boldsymbol{\delta EC} \\ \boldsymbol{\delta OC_u} \\ \boldsymbol{\delta NO_{3u}} \\ \boldsymbol{\delta SO_{4u}} \\ \boldsymbol{\delta OTR_u} \end{bmatrix}, \quad (7)$$

where $\boldsymbol{\rho}_{ij}$ is the submatrix of $\mathbf{K}$, which represents the statistical regression coefficients between the variables i and j (Chen et al., 2013). Note that $\boldsymbol{\rho}_{ij}$is a diagonal matrix with the dimension of model grid points. Each model grid point has a regression coefficient. For convenience, we assumed that the elements of $\boldsymbol{\rho}_{ij}$ is a constant value for all grid points, which are denoted as ρ_{ij} and are calculated by linear regression with all grid points. For example, ρ_{21} can be obtained from the regression equation of OC and EC as

$$\boldsymbol{\delta OC} = \rho_{21}\boldsymbol{\delta EC} + \boldsymbol{\varepsilon}, \quad (8)$$

where $\boldsymbol{\varepsilon}$ is the residual. $\boldsymbol{\delta EC}$ and $\boldsymbol{\delta OC}$ can be estimated from the forecast differences of 24 h forecasts and 48 h forecasts, similar to the statistics of the BEC. Eq. (8) contains the slope but no intercept. The intercept is nearly zero because $\boldsymbol{\delta EC}$ and $\boldsymbol{\delta OC}$ represent forecast differences that can be considered to be zero mean values. After obtaining ρ_{21}, the balanced part (e.g., the value of the regression prediction) of $\boldsymbol{\delta OC}$ can be obtained by

$$\boldsymbol{\delta OC_b} = \widehat{\boldsymbol{\delta OC}} = \rho_{21}\boldsymbol{\delta EC}\,. \quad (9)$$

Where $\widehat{\boldsymbol{\delta OC}}$ represents the predicted value of Eq. (8), which is equal to the balanced part ($\boldsymbol{\delta OC_b}$). Remove the $\boldsymbol{\delta OC_b}$ from the full variables to obtain the unbalanced part ($\boldsymbol{\delta OC_u}$), that is, $\boldsymbol{\varepsilon}$ in Eq. (8). Thus, the calculation of $\boldsymbol{\delta OC_u}$ can be written as

$$\boldsymbol{\delta OC_u} = \boldsymbol{\delta OC} - \rho_{21}\boldsymbol{\delta EC}. \quad (10)$$

Here, $\boldsymbol{\delta OC_u}$ and $\boldsymbol{\delta EC}$ are employed as predictors in the next regression equation to obtain $\boldsymbol{\delta NO_{3b}}$. Then, we can obtain the unbalanced parts of the remaining variables, which are defined as follows:

$$\boldsymbol{\delta NO_{3u}} = \boldsymbol{\delta NO_3} - (\rho_{31}\boldsymbol{\delta EC} + \rho_{32}\boldsymbol{\delta OC_u}), \quad (11)$$

$$\boldsymbol{\delta SO_{4u}} = \boldsymbol{\delta SO_4} - (\rho_{41}\boldsymbol{\delta EC} + \rho_{42}\boldsymbol{\delta OC_u} + \rho_{43}\boldsymbol{\delta NO_{3u}}), \quad (12)$$

$$\boldsymbol{\delta OTR_u} = \boldsymbol{\delta OTR} - (\rho_{51}\boldsymbol{\delta EC} + \rho_{52}\boldsymbol{\delta OC_u} + \rho_{53}\boldsymbol{\delta NO_{3u}} + \rho_{54}\boldsymbol{\delta SO_{4u}}), \quad (13)$$

The coefficient of determination (R^2) can be employed to measure the fit of these regressions. It can be expressed as

$$R^2 = \frac{\mathrm{SSR}}{\mathrm{SST}}, \tag{14}$$

where SSR and SST are the regression sum of squares and the sum of squares for total, respectively.

These unbalanced parts can be considered to be independent because they are residual and random. $\mathbf{B_u}$ denotes the unbalanced variables of the BEC and can be factorized as

$$\mathbf{B_u} = \mathbf{D_u C_u D_u^T}, \tag{15}$$

where $\mathbf{D_u}$ and $\mathbf{C_u}$ are the standard deviation matrix and the correlation matrix, respectively. $\mathbf{C_u}$ should be a block diagonal without cross-correlations as follows:

$$\mathbf{C_u} = \begin{bmatrix} \mathbf{C_{EC}} & & & & \\ & \mathbf{C_{OCu}} & & & \\ & & \mathbf{C_{NO_{3u}}} & & \\ & & & \mathbf{C_{SO_{4u}}} & \\ & & & & \mathbf{C_{OTRu}} \end{bmatrix}. \tag{16}$$

According the definition of the BEC,

$$\mathbf{B} = \langle(\boldsymbol{\delta x})(\boldsymbol{\delta x}^{\mathrm{T}})\rangle. \tag{17}$$

And $\mathbf{B_u}$ can be written as

$$\mathbf{B_u} = \langle(\boldsymbol{\delta x_u})(\boldsymbol{\delta x_u}^{\mathbf{T}})\rangle. \tag{18}$$

Using Eq. (6), Eq. (17) and Eq. (18), the relationship between $\mathbf{B}$ and $\mathbf{B_u}$ is

$$\mathbf{B} = \mathbf{K B_u K^T}. \tag{19}$$

$\mathbf{B^{\frac{1}{2}}}$ and $\mathbf{B_u^{\frac{1}{2}}}$ are defined as the square root of $\mathbf{B}$ and the square root of $\mathbf{B_u}$, respectively. Their transformation is

$$\mathbf{B^{\frac{1}{2}} = K B_u^{\frac{1}{2}}}. \tag{20}$$

Using Eq. (15), Eq. (20) can be written as follows:

$$\mathbf{B^{\frac{1}{2}} = K D_u C_u^{\frac{1}{2}}}. \tag{21}$$

Generally, a transformed cost function of Eq. (2) is expressed as a function of a preconditioned state variable:

$$J(\boldsymbol{\delta z}) = \frac{1}{2}\boldsymbol{\delta z}^T\boldsymbol{\delta z} + \frac{1}{2}\left(\mathbf{H}\mathbf{B}^{\frac{1}{2}}\boldsymbol{\delta z} - \boldsymbol{d}\right)^T \mathbf{R}^{-1}\left(\mathbf{H}\mathbf{B}^{\frac{1}{2}}\boldsymbol{\delta z} - \boldsymbol{d}\right). \quad (22)$$

Here, $\boldsymbol{\delta z} = \mathbf{B}^{-\frac{1}{2}}\boldsymbol{\delta x}$. Using Eq. (21), Eq. (22) can be written as

$$J(\boldsymbol{\delta z}) = \frac{1}{2}\boldsymbol{\delta z}^T\boldsymbol{\delta z} + \frac{1}{2}\left(\mathbf{H}\mathbf{K}\mathbf{D}_\mathbf{u}\mathbf{C}_\mathbf{u}^{\frac{1}{2}}\boldsymbol{\delta z} - \boldsymbol{d}\right)^T \mathbf{R}^{-1}\left(\mathbf{H}\mathbf{K}\mathbf{D}_\mathbf{u}\mathbf{C}_\mathbf{u}^{\frac{1}{2}}\boldsymbol{\delta z} - \boldsymbol{d}\right). \quad (23)$$

Eq. (23) is the last form of the cost function with the cross-correlation of $\mathbf{B}$.

According to Li et al. (2013), the correlation matrix of the unbalanced parts ($\mathbf{C_u}$) is factorized as

$$\mathbf{C_u} = \mathbf{C_{ux}} \otimes \mathbf{C_{uy}} \otimes \mathbf{C_{uz}}. \quad (24)$$

Here, $\otimes$ denotes the Kronecker product, and $\mathbf{C_{ux}}$, $\mathbf{C_{uy}}$ and $\mathbf{C_{uz}}$ represent the correlation matrices between gridpoints in the x direction, the y direction, and the z direction, respectively, with the sizes $n_x \times n_x$, $n_y \times n_y$, and $n_z \times n_z$, respectively. Here, n_x, n_y and n_z represent the numbers of grid points in the x direction, y direction, and z direction, respectively. This factorization can decrease the size of the dimension of $\mathbf{C_u}$. Another desirable property of Eq. (24) is

$$\mathbf{C}_\mathbf{u}^{\frac{1}{2}} = \mathbf{C}_\mathbf{ux}^{\frac{1}{2}} \otimes \mathbf{C}_\mathbf{uy}^{\frac{1}{2}} \otimes \mathbf{C}_\mathbf{uz}^{\frac{1}{2}} \quad (25)$$

$\mathbf{C_{ux}}$ and $\mathbf{C_{uy}}$ are expressed by Gaussian functions, and $\mathbf{C_{uz}}$ is directly computed from the proxy data. They will be discussed in Sec 4.2.

3. WRF/Chem configuration and cross-correlations of emission species

In this section, we describe the configuration of WRF/Chem, whose forecasting products will be employed in the following BEC statistics and data assimilation experiments. In addition, the cross-correlations of emission species from the WRF/Chem emission data are investigated to understand the cross-correlation between different species of the BEC.

3.1 WRF/Chem configuration

WRF/Chem (V3.5.1) is employed in our study. This is a fully coupled online model with a regional meteorological model that is coupled to aerosol and chemistry models (Grell et al., 2005). The model domain with three spatial domains is shown in Figure 1. The horizontal grid spacing for these three domains are 36 km (80×60 points), 12 km (97×97 points), and 4 km (144×96 points), respectively. The outer domain spans southern California and the innermost domain

encompasses Los Angeles. All domains have 31 vertical levels with the top at 50 hPa. The vertical grid is stretched to place the highest resolution in the lower troposphere. The discussion of the BEC and the emissions presented in this paper will be confined to the innermost domain. The initial meteorology conditions for WRF/Chem are prepared using the North American Regional Reanalysis (NARR) (Mesinger et al. 2006). The meteorology boundary conditions and sea surface temperatures are updated at each initialization. For the forecast running, the initial meteorological conditions are obtained from the NARR data. The initial aerosol conditions are obtained from the former forecast. The emissions are derived from the National Emission Inventory 2005 (NEI'05) for both aerosols and trace gases (Guenther et al., 2006). For more details, the readers are referred to Li et al. (2013).

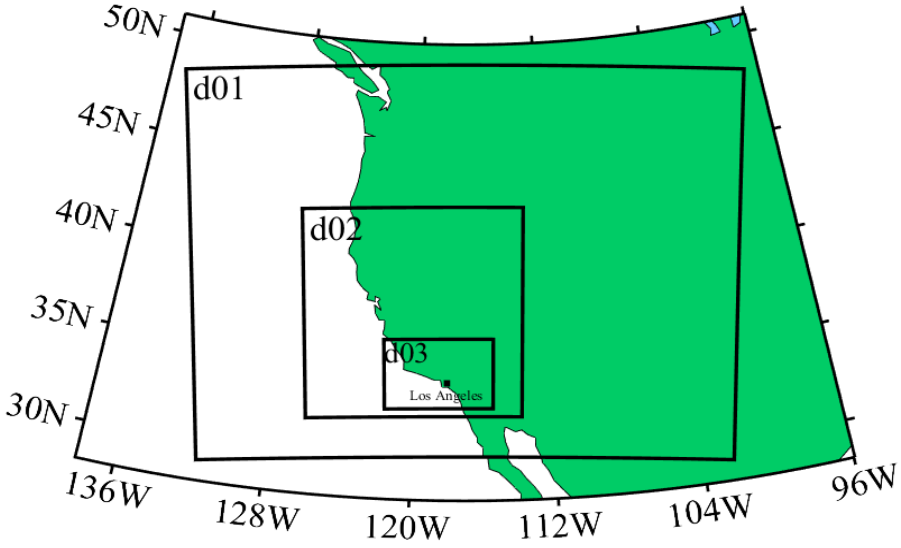

Figure 1. Geographical display of the three-nested model domains. The innermost domain covers the Los Angeles basin; the black point denotes the location of Los Angeles.

3.2 Cross-correlations of emission species

The emission source is necessary for running the WRF/Chem model. It is an important factor for the distribution of the aerosol forecasts. The analysis of the correlations among the emission species can help us to understand the BEC statistics. The emission species is derived from the emission file that is produced by the NEI'05 data for each model domain. Only the emission data for the innermost domain is used to calculate the correlation among the emission species. The emission file contains 37 variables, including gas species and aerosol species. An aerosol species also comprises a nuclei mode and accumulation model species (Peckam et al., 2013). From these

aerosol emission species, five lumped aerosol species are calculated, which is consistent with the variables in the data assimilation. These five lumped species are E_EC (sum of the nuclei mode and the accumulation mode of elemental carbon $PM_{2.5}$), E_ORG (sum of the nuclei mode and the accumulation mode of organic $PM_{2.5}$), E_NO3 (sum of the nuclei mode and the accumulation mode of nitrate $PM_{2.5}$), E_SO4 (sum of the nuclei mode and the accumulation mode of sulfate $PM_{2.5}$), and E_PM25 (sum of the nuclei mode and the accumulation mode of unspeciated primary $PM_{2.5}$).

Figure 2 shows the cross-correlations of the five lumped aerosol emission species. All cross-correlations exceed 0.5. This result reveals that the emission species are correlated, which may be attributed to the common emission sources and diffusion processes that are controlled by the same atmospheric circulation. The most significant cross-correlation is between E_EC and E_ORG with a value of approximately 0.8. This high correlation demonstrates that the emission distributions of these two species are very similar. Their emissions are primary in urban and suburban areas with small emissions in rural areas and along roadways (not shown). As shown in Fig. 2, the lowest cross-correlation is between E_ORG and E_SO4; the latter emissions are primary in the urban and suburban areas with few emissions in rural areas and roadways (not shown).

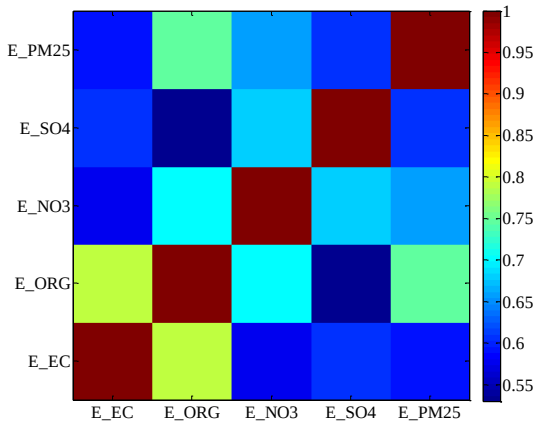

Figure 2. Cross-correlations between emission species of E_EC, E_ORG, E_NO3, E_SO4 and E_PM25. The emission species data are derived from the NEI'05 emissions set for the innermost domain of the WRF/Chem model

4 Balance constraints and BEC statistics

With the configuration of the WRF/Chem model described in Section 3.1, forecasts for one month (from 00UTC of May 15 to 00UTC of June 14, 2010) were performed for the balance constraints and the BEC statistics. Forecast differences between 24 h forecasts and 48 h forecasts are available at 00UTC. Thirty forecast differences are employed as inputs in the NMC method. For this method, 30 forecast differences are sufficient; however, a longer time series may be more beneficial for the BEC statistics (Parrish and Derber, 1992).

4.1 Balance regression statistics

Using the 30 forecast differences between 24 h and 48 h forecasts, we can obtain $\boldsymbol{\delta EC}$, $\boldsymbol{\delta OC}$, $\boldsymbol{\delta NO_3}$ $\boldsymbol{\delta SO_4}$ and $\boldsymbol{\delta OTR}$. The size of these variables is $(N \times 30)$, where N is the number of model grid points. We put these data into Eqs. (6-13) to calculate the regression coefficients of ρ_{ij} and the unbalanced parts of the variables. Note the process of calculation should be step by step, since the latter equation will use the unbalanced parts of former equations. Table 1 shows the regression coefficients whose column and row are consistent with $\rho_{i,j}$ in Eq. (7). The last column in Tab. 1 is the coefficient of determination (R^2) of the regression equations. For the regression equation of OC, the regression coefficient is 0.90 and the coefficient of determination of Eq. (7) is 0.86, which indicates that EC and OC are highly correlated and their mass concentration scales are approximate. Their correlation is similar to the correlation of the stream function and velocity potential; thus, we set them as the first and second variables in the regression statistics. For the regression equation of NO_3, the regression coefficients of EC and OC_u are 4.01 and 3.76, respectively, because the mass concentration scale of NO_3 exceeds the mass concentration scales of EC and OC_u. The coefficient of determination is only 0.32, which indicates that the correlations between NO_3 and EC and between NO_3 and OC_u are weak. This result reveals that the forecast errors of NO_3 differ from the forecast errors of EC and OC_u. A possible reason is that NO_3 is the secondary particle that is primarily derived from the transformation of NO_x, but EC and OC_u are derived from direct emissions. Similar to NO_3, SO_4 is also primarily derived from the transformation of SO_2 and the coefficient of determination for SO_4 is also low. For the last variable OTR, the maximum coefficient of determination is 0.96 because OTR includes some different compositions that are correlated with the first four variables.

Table 1 Regression coefficients of balance operator **K** and the coefficient of determination (regression coefficients correspond to ρ_{ij} in Eq. (7))

species	regression coefficient (ρ)					coefficient of determination (R^2)
EC	1					/
OC	0.90	1				0.86
NO_3	4.01	3.76	1			0.32
SO_4	1.35	-0.21	-3.15	1		0.48
OTR	2.93	2.35	0.28	0.60	1	0.96

Figure 3 shows the cross-correlations of the five full variables and the unbalanced variables. In Fig. 3a, the cross-correlations of the full variables exceed 0.3 and most of them exceed 0.5. In Fig. 3b, however, the cross-correlations of the unbalanced variables are less than 0.2. Some of the cross-correlations are close to zero, which indicates that these unbalanced variables are approximatively independent and can be employed as control variables in the data assimilation system.

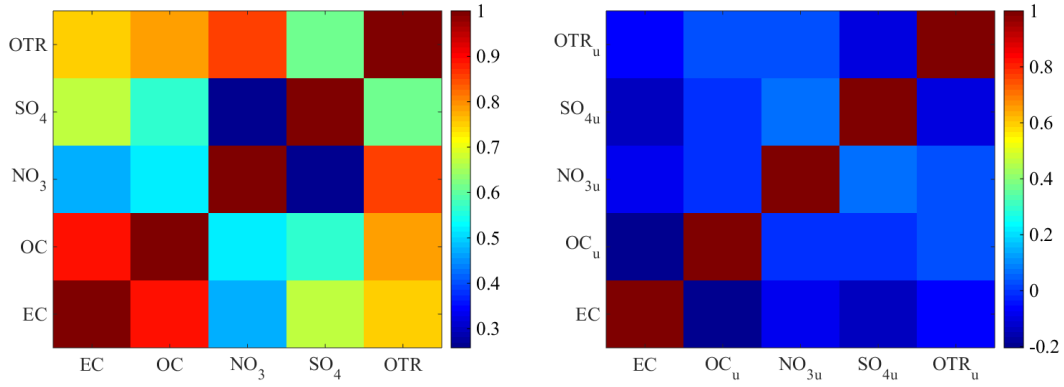

(a) full variables (b) unbalanced variables

Figure 3. Cross-correlations between the five variables of the BEC. These variables are (a) full variables and (b) unbalanced variables of EC, OC, NO_3, SO_4 and OTR.

4.2 BEC statistics

Using the original full variables and the unbalanced variables obtained by the regression equations, the BEC statistics are obtained. Figure 4 shows the vertical profiles of the standard

deviations of the original $\mathbf{D}$ and the unbalanced $\mathbf{D_u}$. In Fig. 4a, the original standard deviation of NO_3 is the largest value, whereas the smallest value is OC, whose profile is close to the profile of EC. All profiles show a significant decrease at approximately 800 m because the aerosol particulates are usually limited under the boundary level. In Fig. 4b, all standard deviations decrease in different degree, with the exception of EC, which remains as the control variable in the unbalanced BEC statistics. Note that the standard deviation of OTR_u decreases by approximately 80% compared with NO_{3u}, which decreases by approximately 10%. This result is attributed to the small coefficient of determination for the regression of NO_3 (in Tab. 1), which indicates that a small portion of NO_3 can be predicted by the regression and a large portion is an unbalanced component. In contrast with NO_3, a small portion of OTR is the unbalanced component.

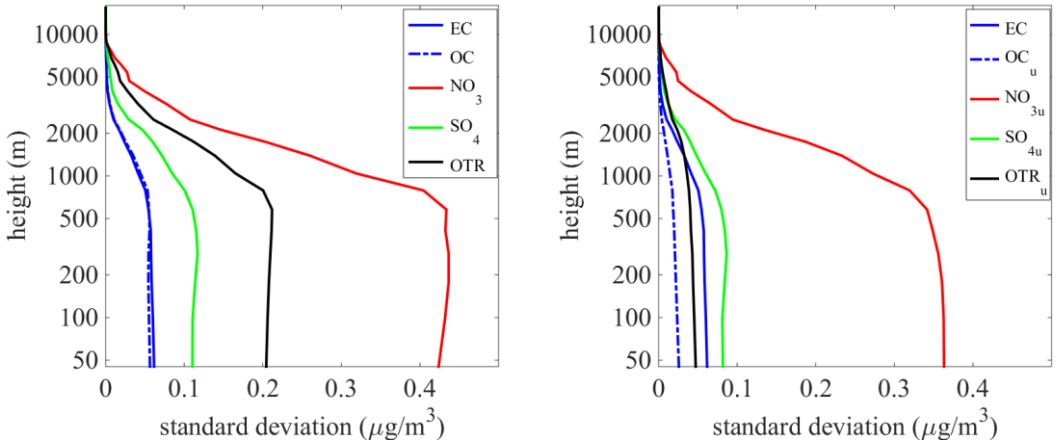

(a) full variables (b) unbalanced variables

Figure 4. Vertical profiles of the standard deviation of the variables. (a) full variables and (b) unbalanced variables

For the correlation matrix of $\mathbf{C}$ and $\mathbf{C_u}$, they are factorized as three independent one-dimensional correlation matrices in Eq. (24). The horizontal correlation $\mathbf{C_x}$ or $\mathbf{C_y}$ is approximately expressed by a Gaussian function. The correlation between two points r_1 and r_2 can be written as $e^{-\frac{(r_2-r_1)^2}{2L_s^2}}$, where L_s is the horizontal correlation scale and is a constant value for $\mathbf{C_x}$ and $\mathbf{C_y}$, which are considered to be isotropic (Li et al., 2013). This scale can be estimated by the curve of the horizontal correlations with distances. Figure 5 shows the curves of the

horizontal correlations for the five control variables. For the full variables (Fig. 5a), the sharpest decrease in the curves is observed for NO_3 and the slowest decrease in the curves is observed for SO_4. We assume that the decline curve is according to the Gaussian function. Then the intersection of the decline curve and the line of $e^{-\frac{1}{2}} (\approx 0.61)$ can be approximately as the value of horizontal correlation scale. The horizontal correlation scales of EC, OC, NO_3, SO_4 and OTR are 25 km, 27 km, 20 km, 30 km and 28 km, respectively. For the unbalanced variables (Fig. 5b), their curves are closer than the curves of the full variables. The correlation scales of EC, OC_u, NO_{3u}, SO_{4u} and OTR_u are 25 km, 23 km, 24 km, 28 km and 25 km, respectively. These results suggest that the unbalanced variables are expressed by some common factors such as EC, OC_u and NO_{3u}, in the regression equations of Eqs. (10-13), which produces consistent horizontal correlation scales.

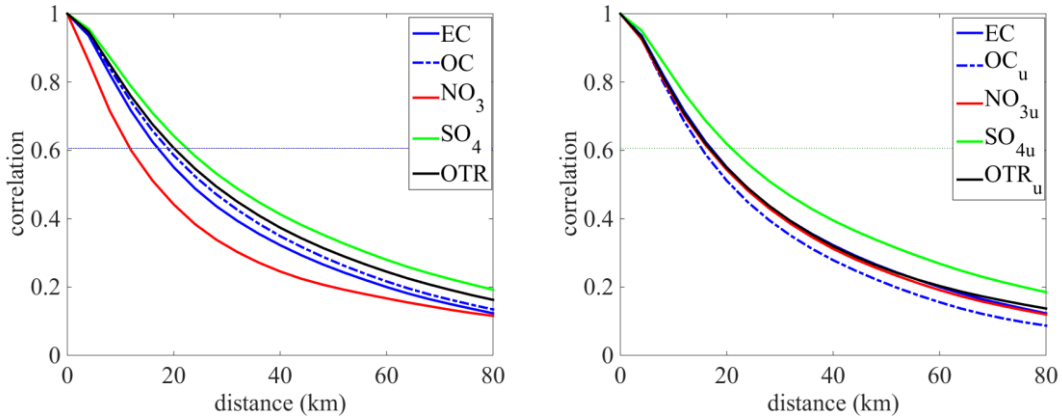

(a) full variables (b) unbalanced variables

Figure 5. Same as Figure 4, with the exception of the horizontal auto-correlation curves of the variables. The horizontal thin line is the reference line of $e^{-\frac{1}{2}} (\approx 0.61)$ for determining the horizontal correlation scales.

For the vertical correlation between $\mathbf{C_z}$ and $\mathbf{C_{uz}}$, they are directly estimated using the forecasting differences in the data assimilation system, but not estimated from a approximately alternative function. Because it is only an $n_z \times n_z$ matrix. Figure 6 shows the vertical correlation matrices $\mathbf{C_z}$ and $\mathbf{C_{uz}}$ for the full variables (left column) and the unbalanced variables (right column), respectively. A common feature of both the full variables and the unbalanced variables is

the significant correlation between the levels of the boundary layer height, which is consistent with the profile of the standard deviation in Fig. 4. Some weak adjustments to the correlations between the full and unbalanced variables are made. For example, the correlation of NO_{3u} is stronger than the correlation of NO_3 between the boundary layers. Similar with the analysis of horizontal correlation scale, the vertical correlation scale of NO_{3u} is larger than the vertical correlation scale of NO_3. Conversely, the vertical correlation scale of OTR_u is smaller than the vertical correlation scale of OTR. These results demonstrate that the vertical correlations for the unbalanced variables are more consistent than the vertical correlations of the full variables, which is similar to the adjustments to the horizontal correlation scale. Note that the differences of vertical correlation are slight, compared with the difference of horizontal. The main reason is that the vertical correlations are generally affected by the atmospheric boundary layer height. Thus, all vertical correlation decreases rapidly for the levels above the boundary layer height.

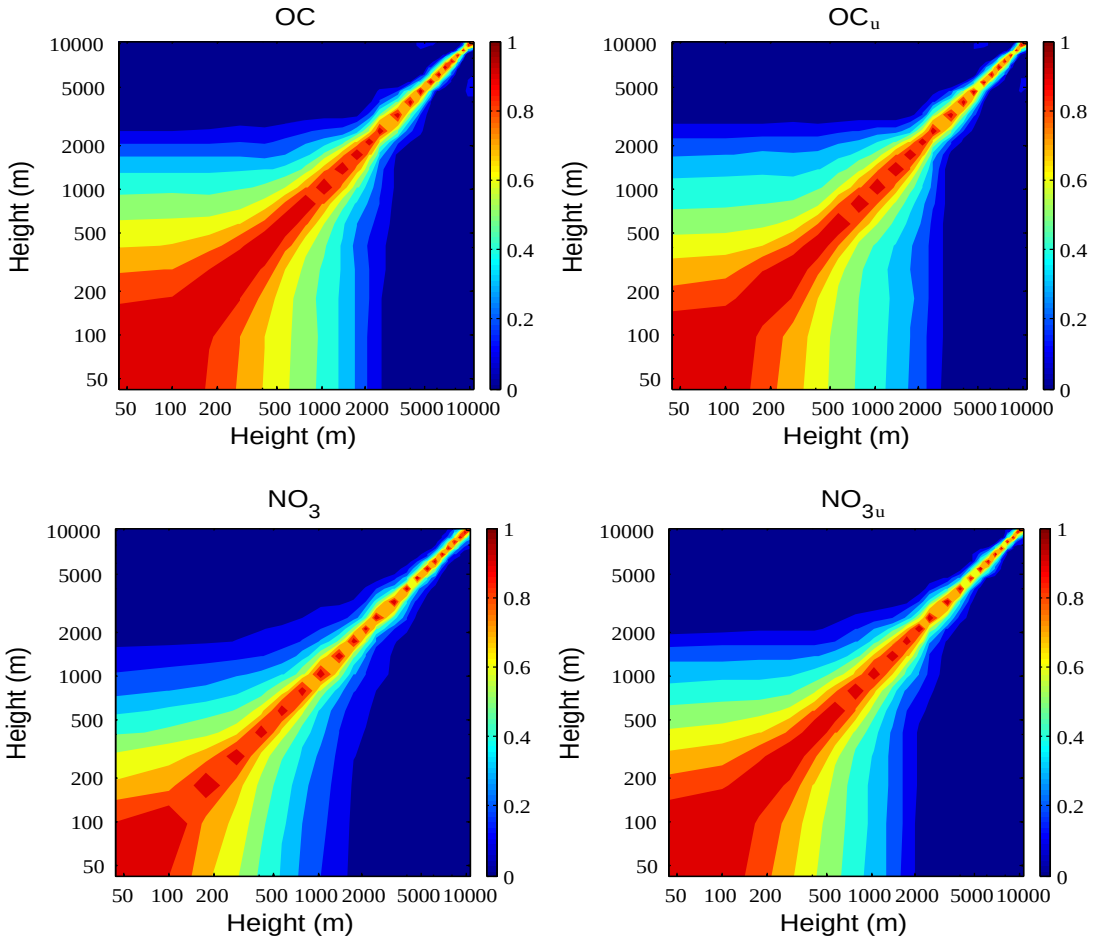

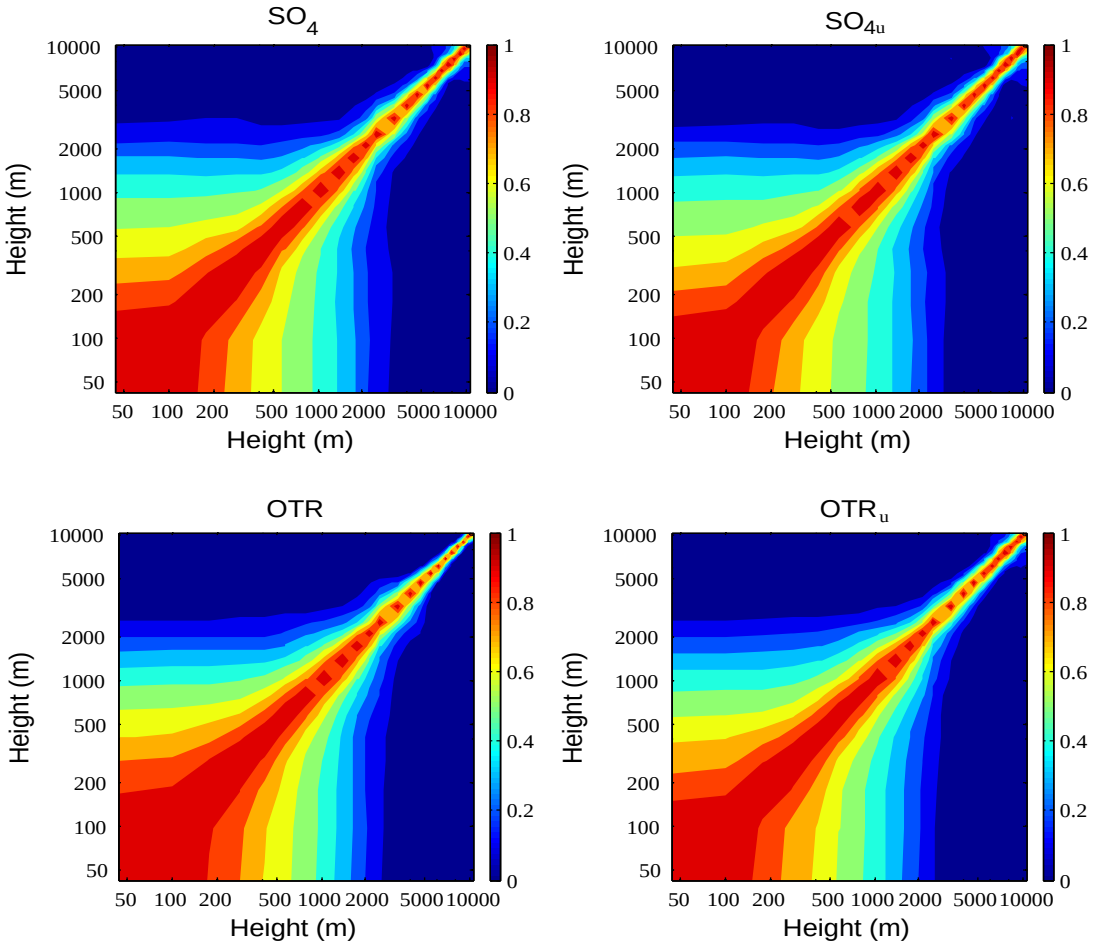

414 Figure 6. Vertical correlations of the five variables of the BEC. The left column represents the full
415 variables, and the right column represents the unbalanced variables.

416

417 **5. Application to data assimilation and prediction**

418 To exhibit the effect of the balance constraint of the BEC, the data assimilation experiments
419 and 24-h forecasts for nine cases are run using WRF/Chem model. The surface $PM_{2.5}$ and
420 aircraft-speciated observations are assimilated using different BEC, and the evaluations are
421 presented for the data assimilation and subsequent forecasts. Three basic statistical measures
422 including mean bias (BIAS), root mean square error (RMSE) and correlation coefficient (CORR)
423 are utilized for the evaluations.

424 **5.1 Observation data and experiment scheme**

425 Two types of observation data are employed in our experiments. The first type of observation
426 data consists of hourly surface $PM_{2.5}$ concentrations from the California Air Resources Board
427 (ARB). There are 42 surface PM2.5 monitoring sites existed in the innermost domain of the

WRF/Chem model (Fig. 7). The second type of observation data is the speciated concentration along the aircraft flight track. The aircraft observations were investigated from the California Research at the Nexus of Air Quality and Climate Change (CalNex) field campaign in 2010. Nine flights data around Los Angeles from 15 May to14 June, 2010 are selected as the cases of data assimilation. Table 2 shows the start time and end time of each flight. The species of the aircraft observations include OC, NO_3, SO_4 and NH_4. Note that NH_4 is not a control variable; thus, the aircraft observation of NH_4 is disregarded in the data assimilation. Because the particle size of the aircraft observations is less than 1.0 μm, some adjustments to the flight observations are made according to the ratios between the concentration under 2.5 μm and the concentration under 1.0 μm for each species using model products. With the ratios multiplied by the aircraft observed concentrations, the speciated concentrations under 2.5 μm can be obtained.

Table 2 The periods of flight during CalNex 2010 and the initial time of assimilation

Number of cases	Start time of flight	End time of flight	Initial time of assimilation
1	18:00 UTC, May 16	01:42 UTC, May 17	00:00 UTC, May 17
2	17:28 UTC, May 19	00:10 UTC, May 20	18:00 UTC, May 19
3	17:28 UTC, May 21	00:10 UTC, May 21	18:00 UTC, May 21
4	23:08 UTC, May 24	05:23 UTC, May 25	00:00 UTC, May 25
5	01:59 UTC, May 30	07:45 UTC, May 30	06:00 UTC, May 30
6	05:00 UTC, May 31	10:54 UTC, May 31	06:00 UTC, May 31
7	07:59 UTC, June 2	14:09 UTC, June 2	12:00 UTC, June 2
8	07:59 UTC, June 3	14:041 UTC, June 3	12:00 UTC, June 3
9	17:56 UTC, June 14	23:35 UTC, June 14	18:00 UTC, June 14

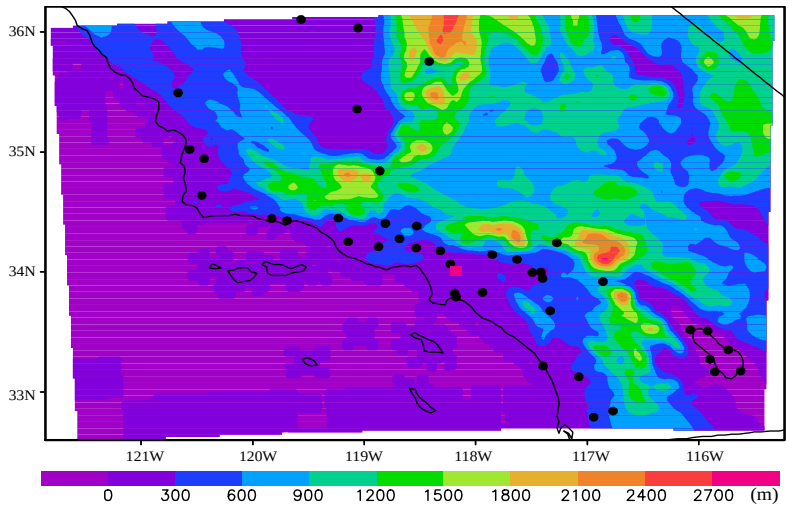

Figure 7. The topography of the innermost domain and the locations of surface monitoring stations (black dots). The red square is the location of Los Angeles

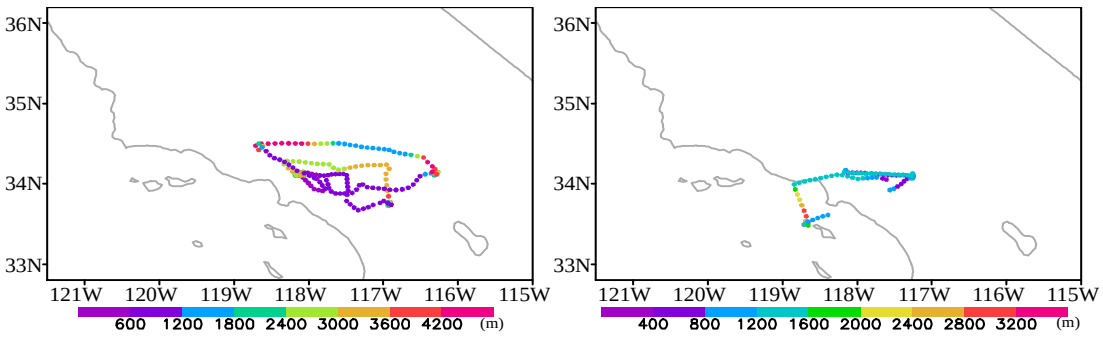

(a) 00:00 UTC±1.5 h, May 17 (b) 18:00 UTC±1.5 h, May 19

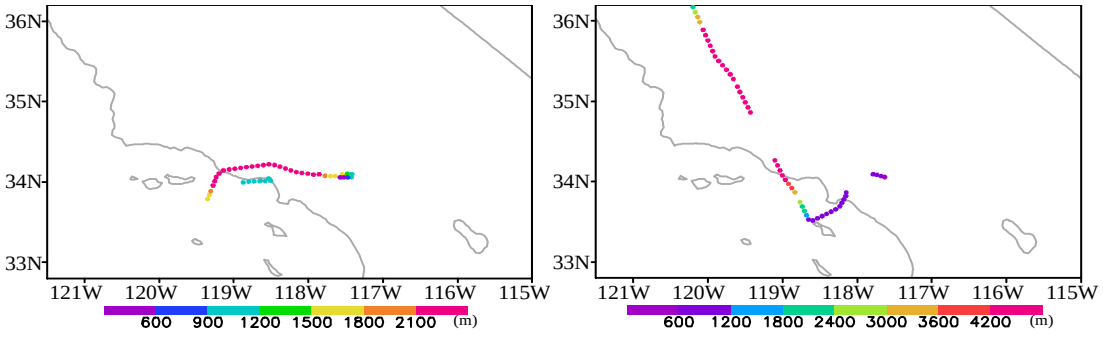

(c) 18:00 UTC±1.5 h, May 21 (d) 00:00 UTC±1.5 h, May 25

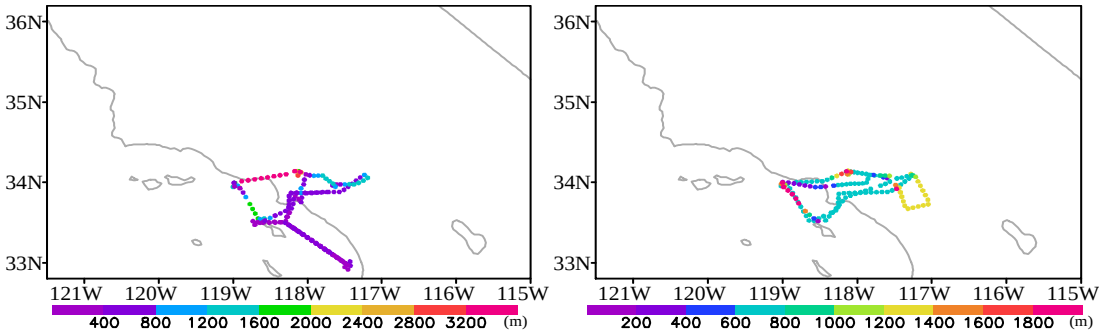

(e) 06:00 UTC±1.5 h, May 30 (f) 06:00 UTC±1.5 h, May 31

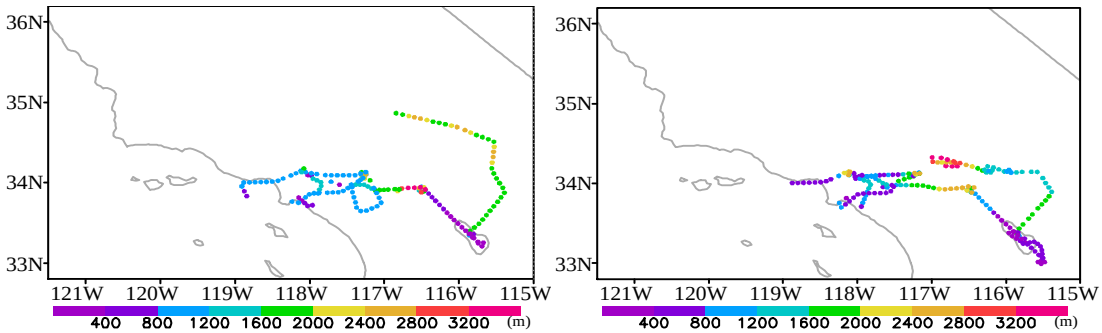

(g) 12:00 UTC±1.5 h, Jun 02 (h) 12:00 UTC±1.5 h, Jun 03

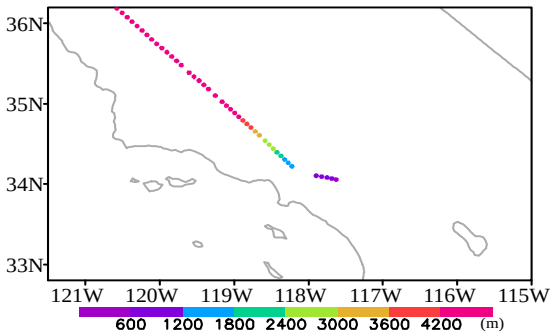

(i) 18:00 UTC±1.5 h, Jun 14

Figure 8. Aircraft flight tracks during the time window of data assimilation for nine cases. The color of the track indicates the aircraft height.

The initial time of data assimilation cases are designed according to the period of flights, showed in Table 2. The time window of assimilation for the flight data is ±1.5h, though some flight times do not completely cover the time windows. Figure 8 shows the aircraft tracks during the time window of data assimilation. It is obvious that the aircarft data on May 21, May 25 and June 14 are relative few as the tracks are almost outside of the study domain. For the surface data, it is only the observations at the initial time are assimilated. For each case, three parallel experiments are performed. The first experiment is the control experiment without aerosol data assimilation, which is frequently known as a free run and denoted as Control. The second experiment is a data assimilation experiment that assimilates surface $PM_{2.5}$ and aircraft observations using the full variables without balance constraints; it is denoted as DA-full. The third experiment is also a data assimilation experiment that also assimilates surface $PM_{2.5}$ and aircraft observations, but employs the unbalanced variables as control variables conducted by the balanced constraint; it is denoted as DA-balance. The backgrounds for DA-full and DA-balance are the forecasting results from the previous runs without DA. These previous forecasting results

have been obtained when we run the model for the BEC statistics. The observation error is the half of standard deviation of the original background variable, and a vertical profile of observation errors is applied with the average profile of standard deviation of the background variable. In each experiment, a 24-h forecasting is run using the WRF/Chem model with the same configuration described in Section 3.1, and the case on June 3, 2010 is presented in detail as an example.

5.2 Increments of data assimilation

Figure 9 shows the horizontal increments of EC, OC, NO_3, SO_4 and OTR at the first model level for the DA-full (left column) and DA-balance experiments (right column) of the case on June 3, 2010. In the DA-full experiment, the increment of EC and OTR (Fig. 9a and 9i) are similar. They are obtained from the surface $PM_{2.5}$ observations because no direct aircraft observations correspond to these two variables. In the DA-balance experiment, significant adjustments are made to the increments of EC (Fig. 9b) under the action of the balance constraints. The observations of OC affect greatly the increments of EC for thee high cross-correlation between EC and OC. Thus the increments of EC are similar with the increments of OC. Similarly, significant adjustments are made to the increment of OTR (Fig. 9j), though there are not the species observation of OTR. There are also some slight adjustments for the increments of OC, NO_3 and SO_4 for the crossing spread among species.

Figure 10 shows the vertical increments along 35.0 N for the DA-full and DA-balance experiments. Similar to Fig. 9, the increments of EC and OTR (Fig. 10a and 10i) spread upward from the surface in the DA-full experiment, which are obtained from the surface $PM_{2.5}$ observation. In the DA-balance, the increments of EC and OTR (Fig. 10b and 10j) exhibit observation information from the aircraft height at approximately 500 m, and the value of the increments show significant increases. The distributions of the increments for these five variables in the DA-balance (Fig. 10, right column) generally tend to coincide compared with the distributions of the increments in the DA-full (Fig. 10, left column). The results of the DA-balance are reasonable due to the influence of each other across the balance constraints.

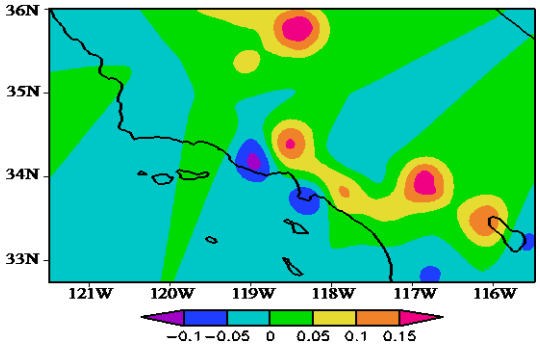

(a) EC in the DA-full

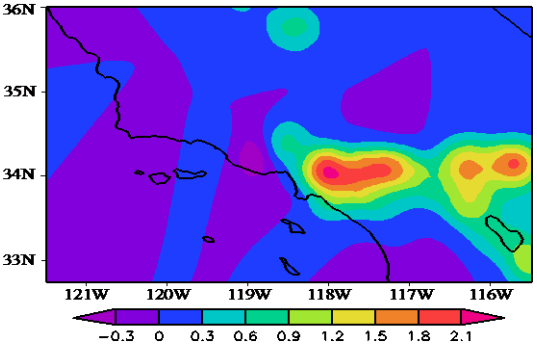

(b) EC in the DA-balance

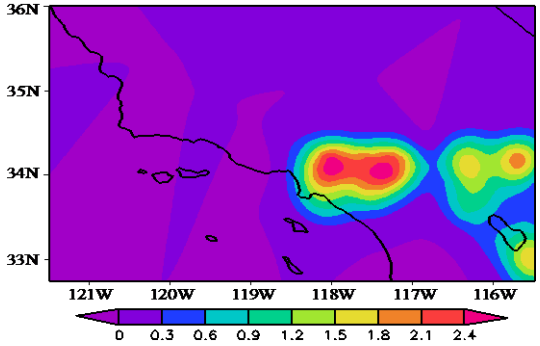

(c) OC in the DA-full

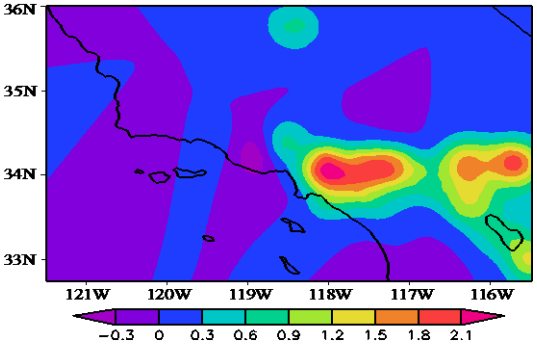

(d) OC in the DA-balance

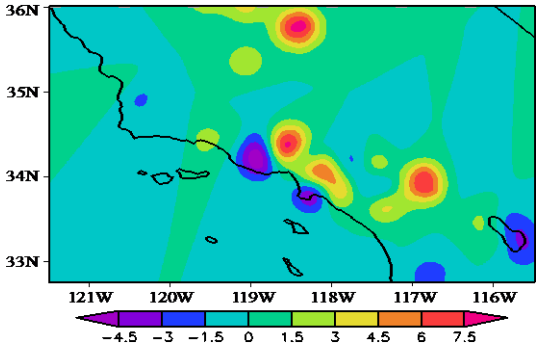

(e) NO_3 in the DA-full

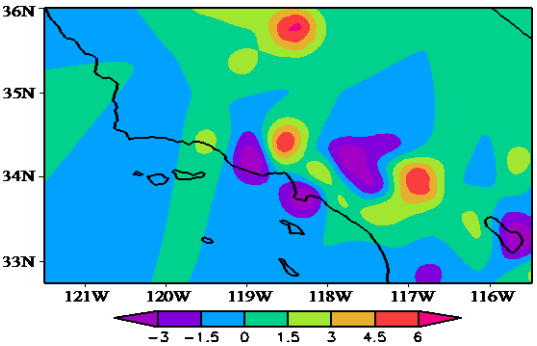

(f) NO_3 in the DA-balance

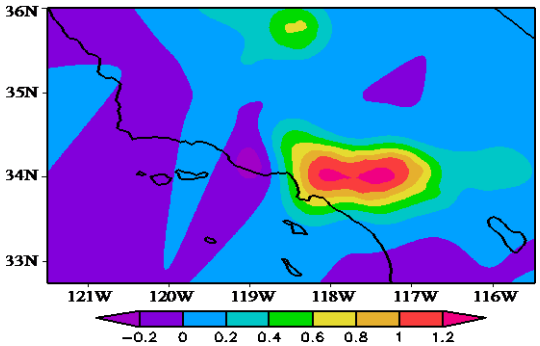

(g) SO_4 in the DA-full

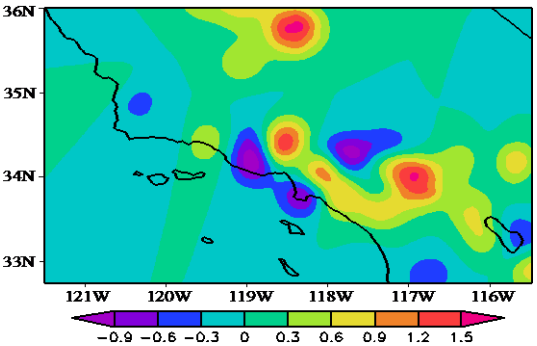

(h) SO_4 in the DA-balance

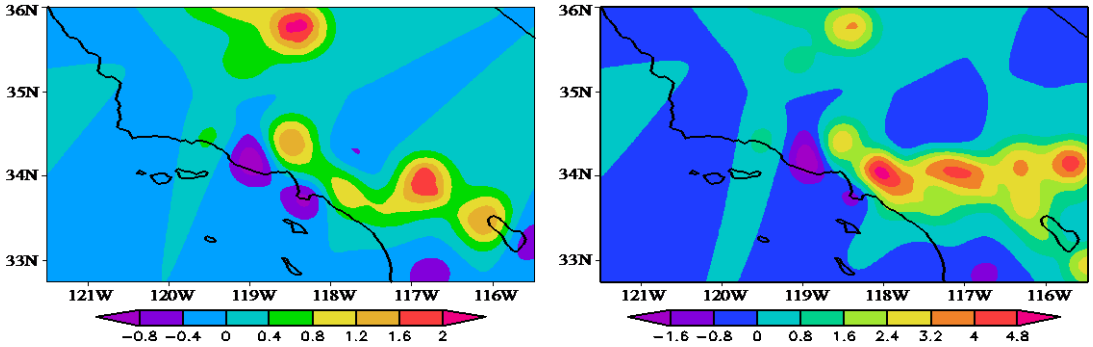

(i) OTR in the DA-full (j) OTR in the DA-balance

499 Figure 9. Surface distributions of increments of the five variables of EC, OC, NO_3, SO_4 and OTR
500 at 12:00 UTC on June 3, 2010. The left column and right column are from DA-full and
501 DA-balance, respectively.
502

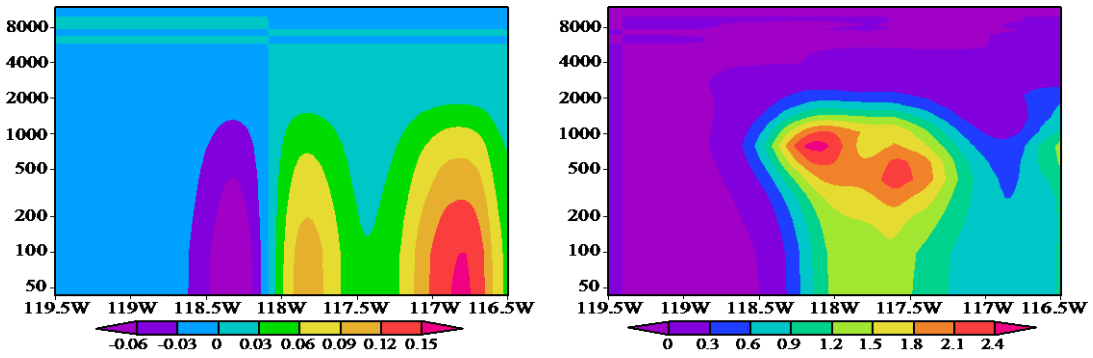

(a) EC in the DA-full (b) EC in the DA-balance

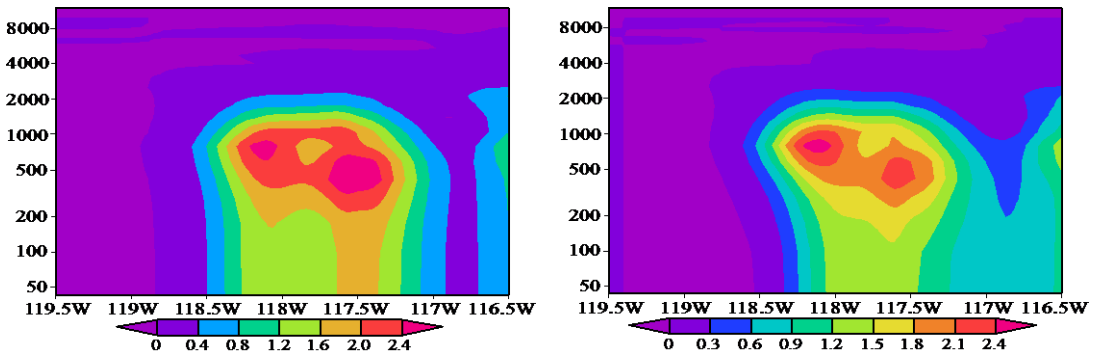

(c) OC in the DA-full (d) OC in the DA-balance

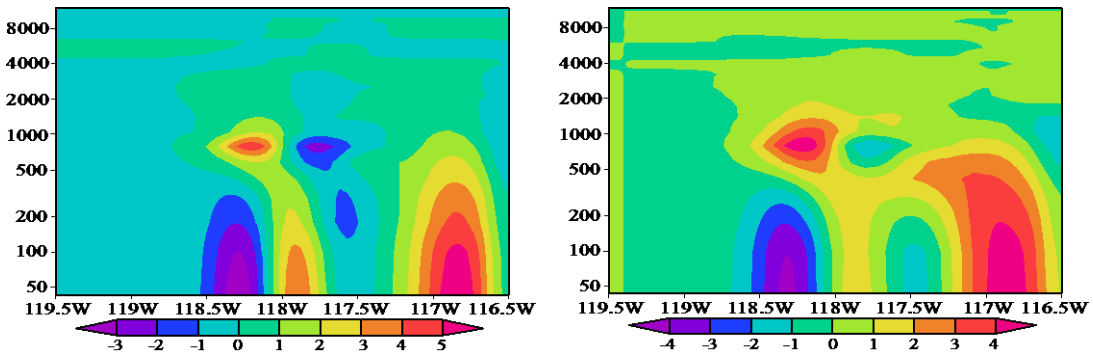

(e) NO_3 in the DA-full (f) NO_3 in the DA-balance

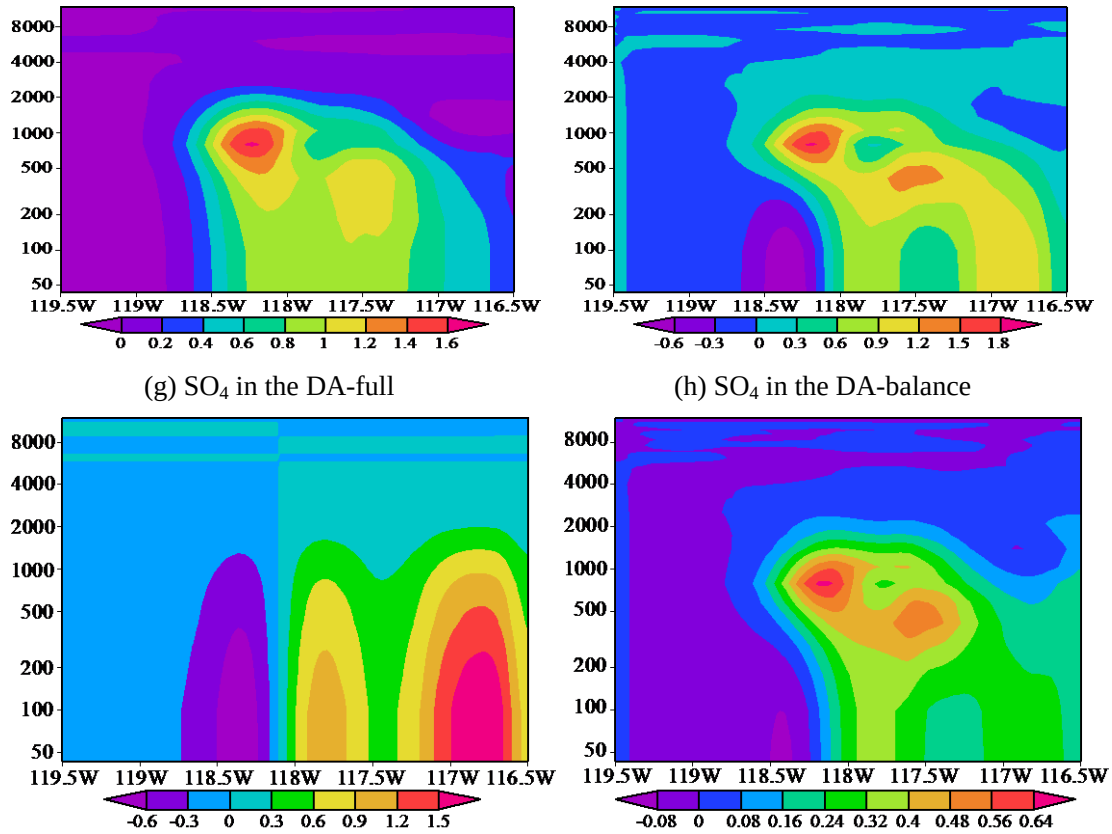

(g) SO_4 in the DA-full (h) SO_4 in the DA-balance

(i) OTR in the DA-full (j) OTR in the DA-balance

Figure 10. Same as Figure 9, with the exception of the vertical sections along 35 N.

5.3 Evaluation of data assimilation and forecasts

Figure 11 shows the scatter plots of the initial model fields versus the surface observation for all nine cases. In Fig. 11a, the simulated concentrations of the Control experiment display a significant underestimation with a BIAS of -3.66 $\mu g/m^3$. The mean concentration of Control is 10.90 $\mu g/m^3$, about 25.1% lower than observed mean concentrations (14.56 $\mu g/m^3$). In the DA-full and DA-balance experiments, there are remarkable increases for the simulated concentrations, and the BIASs reduce to as small as -1.21 and -0.94 $\mu g/m^3$. The RMSE is 9.53 $\mu g/m^3$ in the Control experiment. The RMSE reduces to 4.82 and 4.48 $\mu g/m^3$ in the DA-full and DA-balance experiment, respectively. There are also significant improvements for the CORR in the DA-full and DA-balance experiments, compared with the Control experiment. Furthermore, these three statistical measures of the DA-balance experiments show some slight improvement, compared with that of the DA-full experiments. The result demonstrates that more observation information spread by balance constraints can improve assimilation performance.

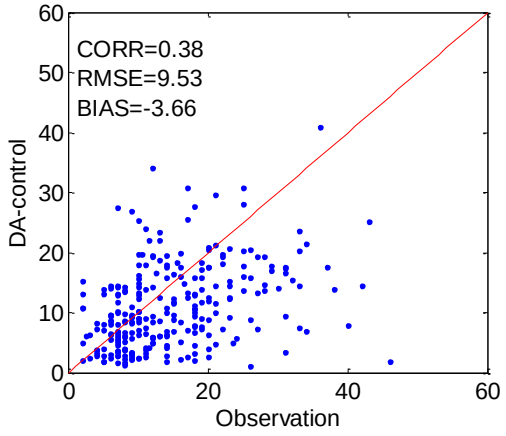

(a) Control

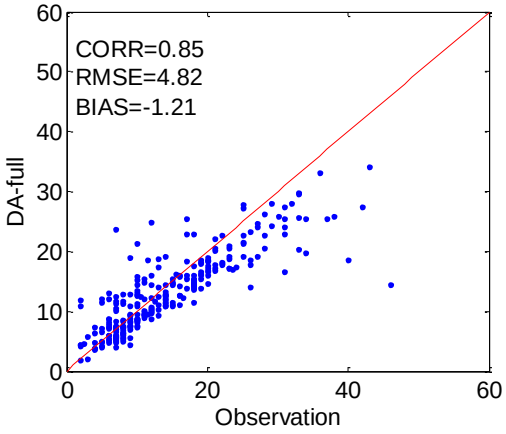

(b) DA-full

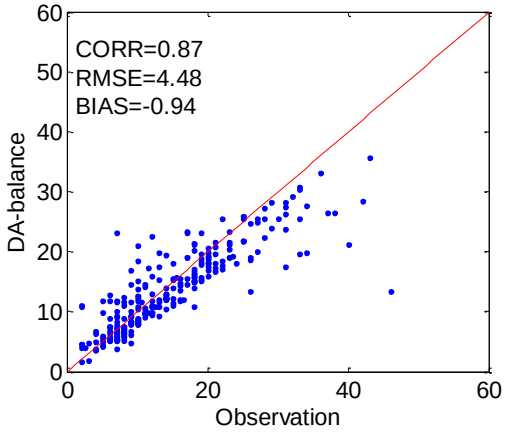

(c) DA-balance

Figure 11. Scatter plots of observed concentrations of $PM_{2.5}$ versus simulated $PM_{2.5}$ concentrations of the experiments of (a) Control, (b) DA-full, and (c) DA-balance for all nine cases.

To evaluate the effects of the data assimilation, the CORR, RMSE and BIAS during the forecast time are calculated for each case, and their averaged results are showed in Figure 12. The CORRs of the DA-balance and DA-full experiments are very close (Fig. 12a). But, the difference increase

after the first hour with a higher CORR in the DA-balance experiment. The CORR of the DA-balance experiment is substantially higher than that of the DA-full experiment from the 2nd hour to the 16th hour. Similar improvements for the RMSE and the BIAS of the DA-balance experiment are observed in Fig. 12b and Fig. 12c, respectively. The improvement for the BIAS in the DA-balance experiment is the most significant among these three statistical measures. The peak value of the improvement for the BIAS (Fig 12c) is at the 4th hour, and the improvement is distinct until the end of forecasts. These improvements indicate that the balance constraint is positive for the subsequent forecasts, which derives from the balanced initial distribution among species.

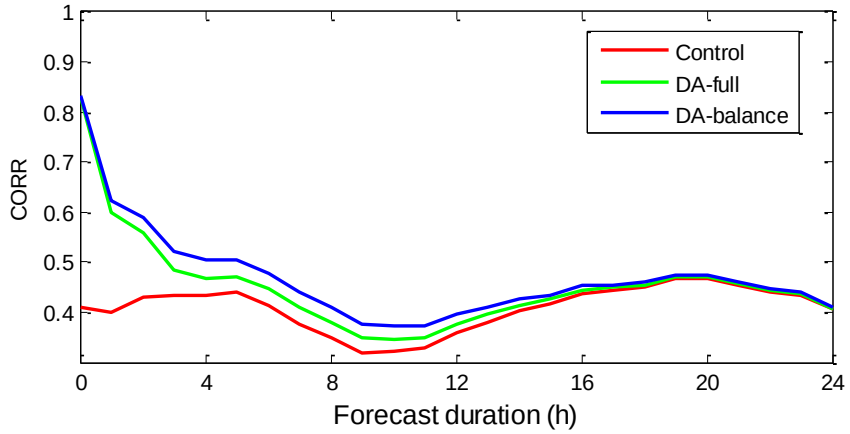

(a) CORR

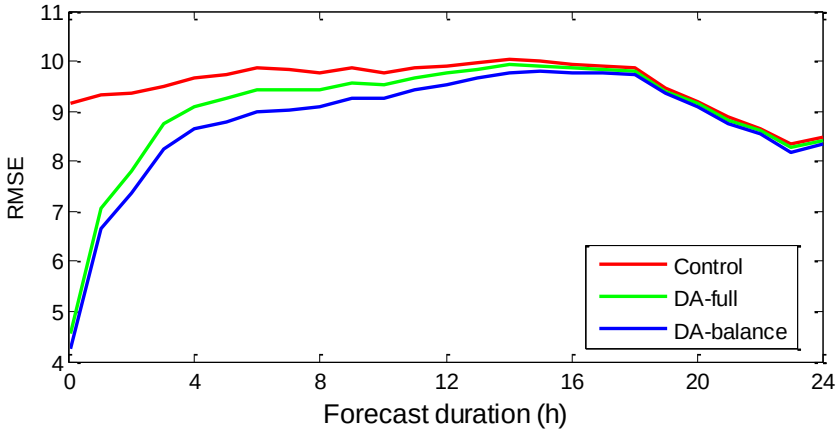

(b) RMSE

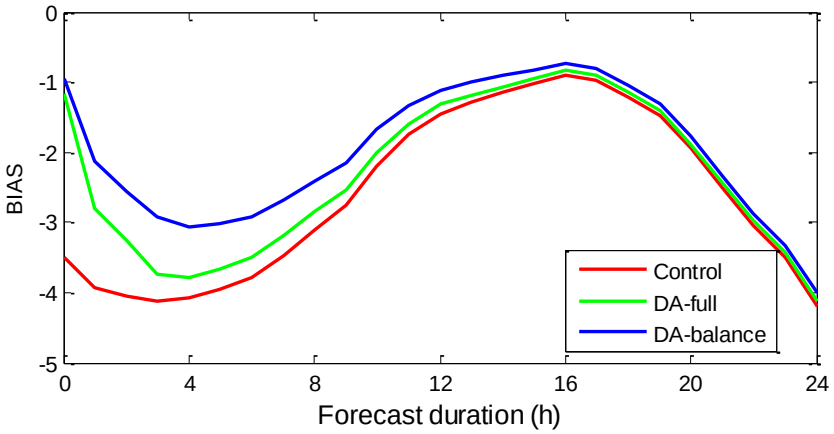

(c) BIAS

Figure 12. The averaged (a) Correlations, (b) root-mean-square errors (RMSE in $\mu g/m^3$) and (c) mean bias (BIAS in $\mu g/m^3$) of the $PM_{2.5}$ concentration forecasts against observations as a function of forecast duration.

6. Summary and discussion

We examined the BEC in a 3DVAR system, which uses five control variables (EC, OC, NO_3, SO_4 and OTR) that are derived from the MOSAIC aerosol scheme in the WRF/Chem model. Based on the NMC method, differences within a month-long period between 24- and 48-h forecasts that are valid at the same time were employed in the estimation and analyses of the BEC. The background errors of these five control variables are highly correlated. Especially between EC and OC, their correlation is as large as 0.9.

A set of balance constraints was developed using a regression technique and incorporated in the BEC to account for the large cross correlations. We employ the the balance constraint to seperate the original full variables into balanced and unbalanced parts. The regression technique is used to express the balanced parts by the unbalanced parts. These unbalanced parts can be assumed independent. Then, the unbalanced parts are employed as control variables in the BEC statics. Accordingly, the standard deviations of these unbalanced variables are less than the standard deviations of the original variables. The horizontal correlation scales of unbalanced variables are closer than that of full variables on the effect of the balance constraints. And the vertical correlations of unbalanced variables show similar trend.

To evaluate the impact of the balance constraints on the analyses and forecasts, three groups of experiments, including a control experiment without data assimilation and two data assimilation

561 experiments with and without balance constraints (DA-full and DA-balance), were performed. In
562 the data assimilation experiments, the observations of surface $PM_{2.5}$ concentration and
563 aircraft-speciated concentration of OC, NO_3 and SO_4 were assimilated. The observations of these
564 three variables can spread to the two remaining variables in the increments of the DA-balance,
565 which results in a more complex distribution. The evaluations of CORR, RMSE and BIAS for the
566 initial analysis fields show more improvement in the DA-balance experiments, compared with the
567 DA-full experiments. Though, these improvement are some slight. An important reason is that the
568 surface $PM_{2.5}$ observations are independent from the aircraft observations. If we evaluate the
569 analysis fields by the species observation of aircraft, there may be more significant improvements
570 in the DA-balance experiments.

571 While the improvements increase after the first forecasting hour in the DA-balance
572 experiments, compared with forecasts of the DA-full experiments. The improvements persist to
573 the end of forecasts, and are substantial from the 2^{nd} hour to the 16^{th} hour (Fig. 12). These results
574 suggested that the balance constraints can serve an import role for continually improving the skill
575 of sequent forecasts. Note that some aircraft data are relative few, and some flight tracks are not
576 around Los Angeles in some cases (Fig. 8). If there are more aircraft observations, the
577 improvements of the DA-balance experiments should be more significant and durable.

578 The developed method for incorporating balance constraints in aerosol data assimilation can
579 be employed in other areas or other applications for different aerosol models. For the aerosol
580 variables in different models, some cross-correlations between different species or size bins
581 should exist because their common emissions and diffusion processes are controlled by the same
582 atmospheric circulation. Although these cross-correlations may be stronger than the
583 cross-correlations of atmospheric or oceanic model variables, theoretic balance constraints, such
584 as geostrophic balance or temperature-salinity balance, do not exist. We expected to discover a
585 universal balance constraint that can describe the physical or chemical balanced relationship of
586 aerosol variables, and utilize it in the data assimilation system. In addition, we expected to expand
587 the balance constraint to include gaseous pollutants, such as nitrite (NO_2), sulfur dioxide (SO_2),
588 and (carbon monoxide) CO. These gaseous pollutants are correlated with some aerosol species,
589 such as NO_3, SO_4 and EC, which can improve the data assimilation analysis fields of aerosols by

assimilating these gaseous observations. The assimilation of aerosol observations may improve the analysis fields of gaseous pollutants.

Code availablity

This data assimilation system is established by ourself. The code of this system can be obtained on request from the first author (zzlqxxy@163.com).

Acknowledgements

This research was supported by the National Natural Science Foundation of China (41275128). We gratefully thank the California Air Resources Board (http://www.arb.ca.gov/homepage.htm) and NOAA Earth System Research Laboratory Chemical Sciences Division (http://esrl.noaa.gov/csd/groups/csd7/measurements/2010calnex/), for providing the download of surface and aircraft aerosol observations.

References

Bannister, R.N., 2008a. A review of forecast error covariance statistics in atmospheric variational data assimilation. I: Characteristics and measurements of forecast error covariances. Quart. J. Roy. Meteor. Soc., 134, 1951–1970.

Bannister, R.N., 2008b. A review of forecast error covariance statistics in atmospheric variational data assimilation. II: Modelling the forecast error covariance statistics. Quart. J. Roy. Meteor. Soc., 134, 1971–1996.

Barker, D.M., Huang, W., Guo, Y.R, Xiao, Q.N., 2004. A Three-Dimensional (3DVAR) data assimilation system for use with MM5: implementation and initial results. Mon. Weather Rev. 132, 897–914.

Benedetti, A., Fisher, M., 2007. Background error statistics for aerosols. Quart. J. Roy. Meteor. Soc., 133, 391–405.

Chen, Y., Rizvi, S., Huang, X., Min, J., Zhang, X., 2013. Balance characteristics of multivariate background error covariances and their impact on analyses and forecasts in tropical and Arctic regions. Meteorol. Atmos. Phys., 121, 79–98.

Cohn, S.E., 1997: Estimation theory for data assimilation problems: Basic conceptual framework

620 and some open questions. J. Meteorol. Soc. Jpn., 75, 257–288.
621 Derber, J., Bouttier, F., 1999. A reformulation of the background error covariance in the ECMWF
622 global data assimilation system. Tellus, 51, 195–221.
623 Geller, M. D., Fine, P. M., and Sioutas, C., 2004. The relationship between real-time and
624 time-integrated coarse (2.5–10m), intermodal (1–2.5m), and fine (<2.5m) particulate matter in the
625 Los Angeles basin. Journal of the Air & Waste Management Association, 54(9), 1029–1039.
626 Grell, G.A., Peckham, S.E., Schmitz, R., McKeen, S.A., Frost, G., Skamarock, W.C., Eder, B.,
627 2005. Fully coupled "online" chemistry within the WRF model. Atmos. Environ., 39, 6957–6976,
628 doi:10.1016/j.atmosenv.2005.04.027.
629 Guenther, A., Karl, T., Harley, P., Wiedinmyer, C., Palmer, P.I., Geron, C., 2006. Estimates of
630 global terrestrial isoprene emissions using MEGAN (Model of Emissions of Gases and Aerosols
631 from Nature). Atmos. Chem. Phys., 6, 3181–3210, doi:10.5194/acp-6-3181-2006.
632 Huang, X.Y., Xiao, Q., Barker, D.M., Zhang, X., Michalakes, J., Huang, W., Henderson, T., 2009.
633 Four-dimensional variational data assimilation for WRF: formulation and preliminary results.
634 Mon. Weather Rev., 137, 299–314.
635 Jazwinski, A. H.,1970. Stochastic processes and filtering theory, Academic Press, New York, 376
636 pp.
637 Kahnert, M., 2008. Variational data analysis of aerosol species in a regional CTM: background
638 error covariance constraint and aerosol optical observation operators. Tellus B, 60(5), 753–770.
639 Li, Z., Zang, Z., Li, Q.B., Chao, Y., Chen, D., Ye, Z., Liu, Y., Liou, K.N., 2013. A
640 three-dimensional variational data assimilation system for multiple aerosol species with
641 WRF/Chem and an application to PM2.5 prediction. Atmos. Chem. Phys., 13, 4265–4278.
642 Liu, Z., Liu, Q., Lin, H.C., Schwartz, C.S., Lee, Y.H., Wang, T., 2011. Three-dimensional
643 variational assimilation of MODIS aerosol optical depth: Implementation and application to a dust
644 storm over East Asia. J. Geophys. Res., 116, D23206, doi:10.1029/2011JD016159.
645 Mesinger, F., DiMego, G., Kalnay, E., Shafran, P., Ebisuzaki, W., Jovic, D., Woollen, J., Mitchell,
646 K., Rogers, E., Ek, M., Fan, Y., Grumbine, R., Higgins, W., Li, H., Lin, Y., Manikin, G., Parrish,
647 D., Shi, W., 2006. North American Regional Reanalysis. B. Am. Meteorol. Soc., 87, 343–360.
648 Peckam, S.E., Grell, G.A., McKeen, S.A., Ahmadov, R., 2013. WRF/Chem Version 3.5 User's
649 Guide. Colrado: NOAA Earth System Research Laboratory.

650 Pagowski, M., Grell, G. A., 2012. Experiments with the assimilation of fine aerosols using an
651 ensemble Kalman filter, J. Geophys. Res., 117, D21302, doi:10.1029/2012JD018333.
652 Pagowski, M., Grell, G.A., McKeen, S.A., Peckham, S.E., Devenyi, D., 2010. Three-dimensional
653 variational data assimilation of ozone and fine particulate matter observations: Some results using
654 the Weather Research and Forecasting–Chemistry model and Grid-point Statistical Interpolation.
655 Q. J. Roy. Meteorol. Soc., 136, 2013–2024, doi:10.1002/qj.700.
656 Parrish, D.F., Derber, J.C., 1992. The national meteorological center spectral statistical
657 interpolation analysis. Mon. Weather Rev., 120, 1747–1763.
658 Ricci, S., Weaver, A.T., 2005. Incorporating State-Dependent Temperature–Salinity Constraints in
659 the Background Error Covariance of Variational Ocean Data Assimilation. Mon. Weather Rev.,
660 133, 317–338.
661 Saide, P.E., Carmichael, G.R., Spak, S.N., Minnis, P., Ayers, J.K., 2012. Improving aerosol
662 distributions below clouds by assimilating satellite-retrieved cloud droplet number. P. Natl. Acad.
663 Sci. USA, 109, 11939–11943, doi:10.1073/pnas.1205877109.
664 Saide, P.E., Carmichael, G.R., Liu, Z., Schwartz, C.S., Lin, H.C., Da Silva, A.M., Hyer, E., 2013.
665 Aerosol optical depth assimilation for a size-resolved sectional model: impacts of observationally
666 constrained, multi-wavelength and fine mode retrievals on regional scale forecasts. Atmos. Chem.
667 Phys., 13, 10425–10444, doi:10.5194/acp-13-10425-2013.
668 Salako, G.O., Hopke, P.K., Cohen, D.D., Begum, B.A., Biswas, S.K., Pandit, G.G., Chung, Y.S.,
669 Rahman, S.A., Hamzah, M.S., Davy, P., Markwitz, A., Shagjjamba, D., Lodoysamba, S.,
670 Wimolwattanapun, W., Bunprapob, S., 2012. Exploring the Variation between EC and BC in a
671 Variety of Locations. Aerosol Air Qual. Res, 12, 1–7.
672 Wu, W.S., Purser, R.J., Parrish, D.F., 2002. Three-dimensional variational analysis with spatially
673 inhomogeneous covariances. Mon. Wea. Rev., 130, 2905-2916
674 Schwartz, C.S., Liu, Z., Lin, H.-C., McKeen, S.A., 2012. Simultaneous three-dimensional
675 variational assimilation of surface fine particulate matter and MODIS aerosol optical depth. J.
676 Geophys. Res., 117, D13202, doi:10.1029/2011JD017383.
677 Schwartz, C. S., Liu, Z., Lin, H.-C., Cetola, J. D., 2014, Assimilating aerosol observations with a
678 “hybrid” variational-ensemble data assimilation system, J. Geophys. Res. Atmos., 119, 4043–4069,
679 doi:10.1002/ 2013JD020937.

Sun C.-H.., Lin Y.-C., Wang C.-S., 2003. 7. Relationships among Particle Fractions of Urban and Non-urban Aerosols. Aerosol and Air Quality Research, 3(1), 7-15.

Zaveri, R.A., Easter, R.C., Fast, J.D., Peters. L K., 2008. Model for Simulating Aerosol Interactions and Chemistry(MOSAIC). J. Geophys. Res., 113, D13204, doi:10.1029/2007JD008782.

Table 1 Regression coefficients of balance operator K and the coefficient of determination (regression coefficients correspond to ρ_{ij} in Eq. (7))

species	regression coefficient (ρ)					coefficient of determination (R^2)
EC	1					/
OC	0.90	1				0.86
NO_3	4.01	3.76	1			0.32
SO_4	1.35	-0.21	-3.15	1		0.48
OTR	2.93	2.35	0.28	0.60	1	0.96

Table 2 The periods of flight during CalNex 2010 and the initial time of assimilation

Number of cases	Start time of flight	End time of flight	Initial time of assimilation
1	18:00 UTC, May 16	01:42 UTC, May 17	00:00 UTC, May 17
2	17:28 UTC, May 19	00:10 UTC, May 20	18:00 UTC, May 19
3	17:28 UTC, May 21	00:10 UTC, May 21	18:00 UTC, May 21
4	23:08 UTC, May 24	05:23 UTC, May 25	00:00 UTC, May 25
5	01:59 UTC, May 30	07:45 UTC, May 30	06:00 UTC, May 30
6	05:00 UTC, May 31	10:54 UTC, May 31	06:00 UTC, May 31
7	07:59 UTC, June 2	14:09 UTC, June 2	12:00 UTC, June 2
8	07:59 UTC, June 3	14:041 UTC, June 3	12:00 UTC, June 3
9	17:56 UTC, June 14	23:35 UTC, June 14	18:00 UTC, June 14

Figure 1 Geographical display of the three-nested model domains. The innermost domain covers the Los Angeles basin; the black point denotes the location of Los Angeles.

Figure 2 Cross-correlations between emission species of E_EC, E_ORG, E_NO3, E_SO4 and E_PM25. The emission species data are derived from the NEI'05 emissions set for the innermost domain of the WRF/Chem model

Figure 3 Cross-correlations between the five variables of the BEC. These variables are (a) full variables and (b) unbalanced variables of EC, OC, NO_3, SO_4 and OTR.

Figure 4 Vertical profiles of the standard deviation of the variables. (a) full variables and (b) unbalanced variables

Figure 5 Same as Figure 4, with the exception of the horizontal auto-correlation curves of the variables. The horizontal thin line is the reference line of $e^{-\frac{1}{2}} (\approx 0.61)$ for determining the horizontal correlation scales.

Figure 6 Vertical correlations of the five variables of the BEC. The left column represents the full variables, and the right column represents the unbalanced variables.

Figure 7 The topography of the innermost domain and the locations of surface monitoring stations (black dots). The red square is the location of Los Angeles

Figure 8 Aircraft flight tracks during the time window of data assimilation for nine cases. The color of the track indicates the aircraft height.

Figure 9 Surface distributions of increments of the five variables of EC, OC, NO_3, SO_4 and OTR at 12:00 UTC on June 3, 2010. The left column and right column are from DA-full and DA-balance, respectively.

Figure 10 Same as Figure 9, with the exception of the vertical sections along 35 N.

Figure 11 Scatter plots of observed concentrations of $PM_{2.5}$ versus simulated $PM_{2.5}$ concentrations of the experiments of (a) Control, (b) DA-full, and (c) DA-balance for all nine cases.

Figure 12 The averaged (a) Correlations, (b) root-mean-square errors (RMSE in $\mu g/m^3$) and (c) mean bias (BIAS in $\mu g/m^3$) of the $PM_{2.5}$ concentration forecasts against observations as a function of forecast duration.